

Anomalous quadrupole transition probabilities in the  $f_{7/2}$  mirror nuclei

R. Escudeiro<sup>1,2</sup> F. Recchia<sup>1,3,\*</sup> N. H. Medina<sup>4</sup> S. M. Lenzi<sup>5</sup> A. Boso<sup>3</sup> P. Aguilera<sup>6</sup> J. Benito<sup>1,3,5</sup> S. Carollo<sup>1,3</sup> A. Goasduff<sup>6</sup> A. Gottardo<sup>6</sup> M. A. Guazzelli<sup>7</sup> J. Ha<sup>8</sup> R. Menegazzo<sup>1</sup> D. R. Napoli<sup>6</sup> R. M. Pérez-Vidal<sup>8,6</sup> J. Pellumaj<sup>1</sup> S. Pigliapoco<sup>1,3</sup> K. Rezykina<sup>1</sup> A. Algora<sup>8</sup> G. de Angelis<sup>6</sup> D. Barrientos<sup>9</sup> P. Bednarczyk<sup>10</sup> G. Benzoni<sup>11</sup> M. Ciemala<sup>10</sup> E. Clement<sup>12</sup> G. De France<sup>12</sup> J. M. Deltoro<sup>13,14</sup> J. Dudouet<sup>15</sup> T. Dupasquier<sup>16</sup> J. Eberth<sup>17</sup> N. Erduran<sup>18</sup> S. Ertürk<sup>19</sup> A. Gadea<sup>8</sup> W. Gelletly<sup>20</sup> V. González<sup>14</sup> H. Hess<sup>17</sup> G. Jaworski<sup>21</sup> M. Jurado<sup>8</sup> W. Korten<sup>22</sup> I. Kuti<sup>23</sup> A. Lefevre<sup>12</sup> F. Legruel<sup>12</sup> A. Lemasson<sup>12</sup> S. Leoni<sup>11,24</sup> J. Ljungvall<sup>25</sup> B. Million<sup>11</sup> J. Nyberg<sup>26</sup> S. E. A. Orrigo<sup>8</sup> M. Palacz<sup>21</sup> Zs. Podolyak<sup>20</sup> A. Pullia<sup>11,24</sup> D. Ralet<sup>12</sup> P. Reiter<sup>17</sup> B. Rubio<sup>8</sup> M. D. Salsac<sup>22</sup> E. Sanchis<sup>27</sup> M. Şenyiğit<sup>28</sup> M. Siciliano<sup>6,22,29</sup> J. Simpson<sup>30</sup> D. Sohler<sup>23</sup> O. Stezowski<sup>15</sup> D. Testov<sup>1</sup> J. J. Valiente-Doboón<sup>13,6</sup> M. Zielńska<sup>22</sup> and R. Wadsworth<sup>31</sup>

<sup>1</sup>INFN, Sezione di Padova, I-35131 Padova, Italy

<sup>2</sup>Department of Physics, KTH Royal Institute of Technology, Stockholm 10691, Sweden

<sup>3</sup>Dipartimento di Fisica e Astronomia dell'Università di Padova, I-35131 Padova, Italy

<sup>4</sup>Instituto de Física da Universidade de São Paulo, São Paulo, Brazil

<sup>5</sup>IPARCOS, Universidad Complutense de Madrid, CEI Moncloa, E-28040 Madrid, Spain

<sup>6</sup>INFN, Laboratori Nazionali di Legnaro, I-35020 Legnaro, Italy

<sup>7</sup>Centro Universitário da FEI, São Bernardo do Campo 09850-901, Brazil

<sup>8</sup>Instituto de Física Corpuscular, CSIC-Universitat de València, E-46071 Valencia, Spain

<sup>9</sup>CERN, CH-1211 Geneva 23, Switzerland

<sup>10</sup>The Henryk Niewodniczański Institute of Nuclear Physics, Polish Academy of Sciences, ulica Radzikowskiego 152, 31-342 Kraków, Poland

<sup>11</sup>INFN, Sezione di Milano, I-20133 Milano, Italy

<sup>12</sup>Grand Accélérateur National d'Ions Lourds (GANIL), CEA/DRF-CNRS/IN2P3, Caen, France

<sup>13</sup>Instituto de Física Corpuscular, CSIC-Universidad de Valencia, 46980 Paterna, Valencia, Spain

<sup>14</sup>Department of Electronic Engineering, University of Valencia, 46100 Burjassot, Valencia, Spain

<sup>15</sup>Université de Lyon, Université Lyon-1, CNRS/IN2P3, UMR5822, IP2I, 4 Rue Enrico Fermi, F-69622 Villeurbanne Cedex, France

<sup>16</sup>Université Lyon 1, CNRS/IN2P3, IPN-Lyon, F-69622 Villeurbanne, France

<sup>17</sup>Institut für Kernphysik, Universität zu Köln, Zùlpicher Strasse 77, D-50937 Köln, Germany

<sup>18</sup>Faculty of Engineering and Natural Sciences, Istanbul Sabahattin Zaim University, 34303 Istanbul, Turkey

<sup>19</sup>Department of Biophysics, Faculty of Medicine, Nigde Omer Halisdemir University, 51200 Nigde, Turkey

<sup>20</sup>Department of Physics, University of Surrey, Guildford GU27XH, United Kingdom

<sup>21</sup>Heavy Ion Laboratory, University of Warsaw, 02-093 Warsaw, Poland

<sup>22</sup>IRFU, CEA, Université Paris-Saclay, F-91191 Gif-sur-Yvette, France

<sup>23</sup>HUN-REN Institute for Nuclear Research (ATOMKI), H-4026 Debrecen, Hungary

<sup>24</sup>Dipartimento di Fisica, Università di Milano, I-20133 Milano, Italy

<sup>25</sup>Université Paris-Saclay, CNRS/IN2P3, IJCLab, 91405 Orsay, France

<sup>26</sup>Department of Physics and Astronomy, Uppsala University, SE-75120 Uppsala, Sweden

<sup>27</sup>Departamento de Ingeniería Electrónica, Universitat de València, 46100 Burjassot, Valencia, Spain

<sup>28</sup>Department of Physics, Ankara University, 06100 Besevler, Ankara, Turkey

<sup>29</sup>Physics Division, Argonne National Laboratory, Lemont, Illinois 60439, USA

<sup>30</sup>STFC Daresbury Laboratory, Daresbury, Warrington WA44AD, United Kingdom

<sup>31</sup>School of Physics, Engineering and Technology, University of York, Heslington, York YO10 5DD, United Kingdom



(Received 19 September 2025; revised 2 February 2026; accepted 27 February 2026; published 3 April 2026)

Lifetimes of several excited states in the mirror nuclei  $^{47}\text{Cr}$  -  $^{47}\text{V}$  and  $^{49}\text{Mn}$  -  $^{49}\text{Cr}$ , located at the center of the  $f_{7/2}$  shell, were measured using the advanced  $\gamma$ -ray tracking array AGATA. The Doppler shift attenuation method was employed to determine such lifetimes in the subpicosecond range. The reduced transition probabilities obtained from the lifetimes are compared to shell-model calculations in the full  $fp$  space. The shell-model-calculated  $B(E2)$  values were underestimated in comparison with experimental data. In particular,

\* Contact author: francesco.recchia@unipd.it

large discrepancies are obtained in  $^{49}\text{Mn}$  at low spin. These results suggest an incomplete understanding of low-energy states in the studied nuclei and call for further refinement of the existing nuclear structure theories.

DOI: [10.1103/1gt6-nc12](https://doi.org/10.1103/1gt6-nc12)

## I. INTRODUCTION

The experimental measurement of electromagnetic transition probabilities between nuclear-bound states is a well-established tool to probe the structure of nuclei. In particular, the measurement of  $E2$  transition probabilities allows us to infer information about intrinsic quadrupole moments and deformation. The radiative transition strength can be obtained from the overlap of the initial and final state through an interaction that is obtained by integrating over the radial coordinate the product of the vector potential and the nuclear current density [1]. In the nuclear current density, both neutrons and protons contribute separately, and their contribution can be formalized in terms of a sum of isovector and isoscalar components. This formalism allows the derivation of several selection rules; see, for example, Morpurgo [2], Radicati [3], and Gell-Mann *et al.* [4].

Moreover, the separation of the  $E2$  transition strength into isoscalar and isovector components sets the basis for a formal interpretation of the effective charges commonly used in shell-model calculations to obtain a realistic estimation for the radiative transition probabilities. In fact, shell-model calculations are limited to a valence space where a limited number of nucleons can interact. If in the calculation, the charges of protons and neutrons are replaced by effective values, a realistic estimation for the transition probabilities can be obtained. As explained by Federman and Zamick [5], such effective values might be understood in terms of the polarization of the core used for the shell-model calculation. Different sets of effective charges for protons and neutrons have been proposed [6–8]. For these cases, the isoscalar charge is dominant over the isovector charge.

In the experiment here reported, we compare the quadrupole transition probabilities in two pairs of mirror nuclei in the  $f_{7/2}$  shell. In the proton-rich mirror nucleus, the isoscalar and the isovector components concur coherently, while in its mirror nucleus, the isovector contributes with an opposite sign. The comparison of transition probabilities in the two mirror nuclei allows us to evaluate the contribution of each component.

Assuming charge independence, the transition probabilities of the isospin analog states can be used to decompose the electric quadrupole matrix element into the proton  $M_{\pi}$  and the neutron  $M_{\nu}$  contributions. This was proposed [9] as a method to obtain precision measurements of  $M_{\nu}$ . It can be used to validate, for example, hadron inelastic scattering, for which the effective interaction between the probe and the bound nucleons must be expressed in the form of single-body operators.

Brown and collaborators [10] systematically studied  $sd$ -shell nuclei. From the comparison of  $T = 1/2$  and  $T = 1$  mirror nuclei, the dominance of the isoscalar component could be highlighted, and different dependencies could be stud-

ied. Further analysis on these  $sd$ -shell nuclei performed by Alexander and collaborators [11] could show that the isoscalar effective charge  $e_{1S}$  increases linearly with the number of nucleons in the valence space, while the isovector part decreases. More recently, Stroberg and collaborators [12] revisited the  $sd$ -shell nuclei, systematically comparing the experimental  $E2$  strength with the ones obtained with the valence-space in-medium similarity renormalization group method (VS-IMSRG) and with shell-model calculations. The VS-IMSRG method resulted in an underestimation of the strength values, but the conclusion of Stroberg *et al.* [12], like previous studies, showed dominance of the isoscalar character, indicating the independence of the isospin for the studied nuclei.

The study of the nuclear deformation in the  $f_{7/2}$  shell, between  $^{40}\text{Ca}$  and  $^{56}\text{Ni}$ , played a fundamental role in developing the understanding of nuclear structure. The shell-model description for nuclei in the middle of the  $fp$  shell has achieved remarkable success, being capable of reproducing in great detail their level schemes using adequate effective interactions such as KB3G [13], specifically tuned for this mass region. Mirror symmetry has been exploited in several of these nuclei to highlight the microscopic mechanism at play to construct spin along the *yrast* line of nuclei in this mass region. These studies also allow us to obtain information on shape and radius changes with increasing angular momentum, as well as the detailed microscopic configuration of the wave functions, thus providing a consistent and detailed description of this portion of the nuclear chart. Such investigations have been carried out with systematic studies of mirror energy differences in isospin doublets and triplet energy differences for  $T = 1$  nuclei [14]. Although excitation energies have been measured and compared between mirror nuclei, the information on level lifetimes, and consequently transition probabilities, is still limited to certain states experimentally accessed. Fusion-evaporation reactions offer the experimental opportunity to extend such investigations toward the high-spin states. When both mirror nuclei are measured in the same experiment, systematic errors cancel out and differences between the lifetimes of the mirror system can be properly highlighted, obtaining in this way a more reliable estimation for isoscalar and isovector components contributing to the composition of the transition probabilities.

Cameron and collaborators studied the mirror energy differences (MED), in the mirror pair  $^{47}\text{Cr} - ^{47}\text{V}$  [15]. Shell-model calculations including charge-symmetry breaking and the Coulomb interaction were able to reproduce these data [8,14]. The lifetimes of three excited states in the  $^{47}\text{Cr}$  were determined by Tonev and collaborators using the Doppler shift attenuation method [16]. In this work, the lifetime measurement is being revisited to evaluate the properties of the mirror pair. To minimize systematic errors and cross-check the method, the well-known lifetimes of excited states of its

mirror,  $^{47}\text{V}$ , have also been measured. Mirror energy differences in the mirror pair  $^{49}\text{Mn}$  -  $^{49}\text{Cr}$  were first studied in 1990 by Cameron *et al.*, in which the mirror symmetries up to  $J^\pi = 19/2^-$  were studied [17,18]. In this study, the authors related the energy differences of the isobaric analog states (IAS) to the different nucleon alignments. When this mirror pair was revisited by O'Leary *et al.* in 1997, the mirror symmetry was studied up to the band termination at  $J^\pi = 31/2^-$  [19]. It was shown how the nuclei generate their angular momentum, from collective rotational motion to a full alignment of the angular momentum vectors of the valence nucleons. In 2015, Bentley and collaborators [20] used this and other  $fp$ -shell mirror pairs to determine the  $J$  dependency of the isospin nonconserving matrix elements. This mirror pair is being revisited in the present work to determine the lifetime of four excited states in  $^{49}\text{Mn}$  for the first time. The well-known lifetimes of the IAS in the  $^{49}\text{Cr}$  were also measured simultaneously to minimize systematic errors and cross-check the method.

## II. EXPERIMENTAL DETAILS AND DATA ANALYSIS

An experiment to populate excited states in  $^{47}\text{Cr}$  and  $^{49}\text{Mn}$  and their mirror nuclei,  $^{47}\text{V}$  and  $^{49}\text{Cr}$ , has been performed at GANIL Laboratory, using a fusion-evaporation reaction in which a 115-MeV  $^{36}\text{Ar}$  beam bombarded a  $550\ \mu\text{g}/\text{cm}^2$  CaO target with a  $10\ \text{mg}/\text{cm}^2$  gold backing. The majority of the fusion reactions occurred with the oxygen present in the target. The  $\gamma$  rays from the populated nuclei were detected using the advanced gamma tracking array (AGATA) spectrometer [21,22], composed, during this campaign, of 36 tapered highly segmented high-purity germanium crystals arranged at backwards angles ranging from  $110^\circ$  to  $160^\circ$  to the beam direction. The reaction channels were selected by detecting the evaporated particles from the compound nucleus, using two sets of ancillary detectors. The light-charged particles were detected using DIAMANT [23,24] implemented for this campaign with 56 CsI(Tl) scintillators arranged around the target in the reaction chamber. The evaporated neutrons were detected using the neutron detector array (NEDA) [25] and neutron wall [26] detectors, composed of liquid scintillators. The detection efficiencies achieved for the ancillary devices were 40(1)% for proton detection, 26(6)% for  $\alpha$  particles, and 26(7)% for neutrons. These efficiency values were obtained keeping the probability of particle misidentification below 0.1%.

The events were recorded using  $\gamma$ - $\gamma$  or  $\gamma$ -neutron trigger conditions, for a total of  $\approx 10^{10}$   $\gamma$ - $\gamma$  coincidence events. However, for the observation of  $\gamma$ -rays depopulating weak exit channels, multiple-particle coincidences were required. The reaction channel selection has been achieved by sorting the data into particle-gated  $\gamma$ - $\gamma$  matrices. Calculations performed with the fusion-evaporation pace code [27] predicted population cross sections of approximately 6 mb for the  $^{47}\text{Cr}$   $\alpha n$  channel and 1 mb for the  $^{49}\text{Mn}$   $p2n$  channel, while predicting for their mirrors 150 mb for the  $^{47}\text{V}$   $\alpha p$  channel and 350 mb for the  $^{49}\text{Cr}$   $p2n$  channel.

In order to determine excited-state lifetimes, the Doppler shift attenuation method (DSAM) was applied [28,29]. This method relies on the fact that the Doppler effect is attenuated

as the residual nuclei are slowing down inside the stopping material, broadening and shifting the  $\gamma$ -ray energy peaks in the spectrum due to the velocity difference of the  $\gamma$ -ray emitting nuclei. The shifted amount depends on the level lifetime, the observation angle, the target composition and thickness, and the lifetimes and intensities of the feeding transitions. Missing intensities coming from unobserved feeding transitions must be taken into account and are called side-feeding transitions. The DSAM utilizes the peak shape of the Doppler-shifted  $\gamma$ -ray transitions to obtain the lifetime of a nuclear level, since the lifetime of a particular level  $L$  is related to its feeding rates. If the line shapes of the feeding transitions are known, the rate can be unfolded and the level lifetime can be deduced [30]. In this work, the Doppler-shifted  $\gamma$ -ray transitions were analyzed with the AGATA code [31] based on geant4 Monte Carlo simulations, which considers the passage of particles through matter and can simulate the response function of the entire array [32]. Several simulations of the full  $\gamma$ -ray spectrum were performed until achieving the minimum  $\chi^2$ . A total of  $2 \times 10^7$  events were simulated, aiming to reproduce the observed  $\gamma$ -ray spectrum. This approach relies on information about the nuclear reaction, the experimental  $\gamma$ -ray spectrum, the AGATA geometry, the level scheme, and the  $\gamma$ -ray intensities extracted from the experimental spectra to determine the lifetimes by reproducing the observed line shapes. The starting lifetime values for the adopted grid-search algorithm were obtained using the lineshape set of programs, usually used for DSAM lifetime determination using Compton-suppressed  $\gamma$ -detector arrays [33,34].

The spectra containing the Doppler-shifted  $\gamma$ -ray transitions were created by gating on the lowermost *yrast* transition observed for each nucleus in their corresponding particle-restricted  $\gamma$ - $\gamma$  matrices. The gate in the transition above (GTA) or the narrow gate in the transition below (NGTB) could not be applied due to limited statistics in the  $^{47}\text{Cr}$  and  $^{49}\text{Mn}$  channels of interest. In all cases, the energy of the  $\gamma$ -rays shown in the level scheme was obtained from the present experiment, while the spin assignment and the order of the levels have been taken from the literature. To perform this type of analysis, the lifetime of the highest level in the level scheme with observable  $\gamma$ -ray transitions needs to be obtained first, as its feeding times affect the line shape of the  $\gamma$ -ray transitions depopulating the lower levels. The lack of knowledge of the feeding transitions for the uppermost populated level requires the modeling of its feeding patterns, meaning that the lifetime for such a level cannot be obtained free of systematic errors, being called an effective lifetime [30,35]. Once the lifetime for the uppermost level in a cascade is determined, the lifetime of the levels below it in the cascade can be obtained.

### A. Analysis of the mirror pair $A = 47$

The  $\gamma$ -rays depopulating the  $(23/2^-)$ ,  $(19/2^-)$ , and  $(15/2^-)$  excited states of  $^{47}\text{Cr}$  exhibited a Doppler shift. The partial level scheme adopted for  $^{47}\text{Cr}$  is shown in Fig. 1(a). The energy of the observed  $\gamma$ -ray depopulating the  $(23/2^-)$  level is 1766 keV. This  $\gamma$ -ray is emitted from the uppermost populated level in the 99-keV-gated spectrum. In all cases, the feeding times from the continuum were considered to be

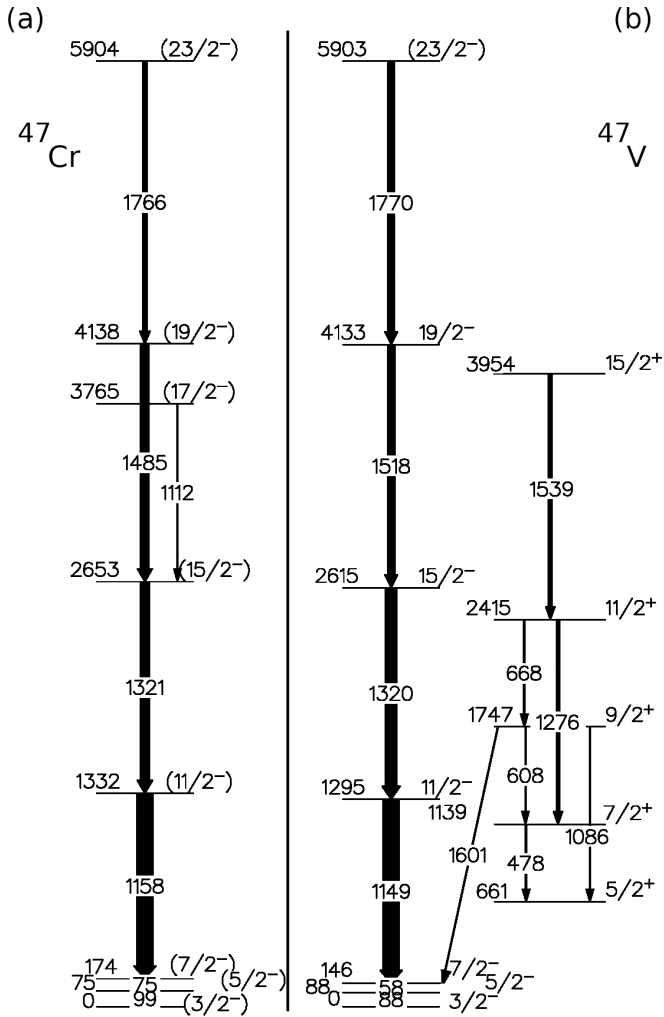


FIG. 1. (a) Partial level scheme for  $^{47}\text{Cr}$ . (b) Partial level scheme for  $^{47}\text{V}$ . The schemes include the levels in which  $\gamma$ -ray transitions were used in the determination of the excited-state lifetimes.

relatively fast, with a transition lifetime of  $\tau = 0.2$  ps [36]. Other stopped peaks on the Doppler-shifted tail of the 1766-keV transition were added to improve the quality of the fit

with the results that can be observed in Fig. 2(a). The lifetime of the (19/2<sup>-</sup>) excited state was obtained using the line shape of the 1485-keV  $\gamma$ -ray, (19/2<sup>-</sup>) → (15/2<sup>-</sup>). This level is fed by the 1766-keV transition and a side feeding transition to account for the missing intensity, and the resulting fit can be observed in Fig. 2(b). The lifetime of (15/2<sup>-</sup>) was obtained using the 1321-keV  $\gamma$ -ray transition, (15/2<sup>-</sup>) → (11/2<sup>-</sup>). The fits performed using the AGATA geant4 code are shown in Fig. 2. The  $\gamma$ -ray transition depopulating (11/2<sup>-</sup>) does not present a significant Doppler shift, and thus the DSAM cannot be applied. A lower limit of 3 ps is assigned to the lifetime of this state, considering that the average stopping time of the recoil nuclei in the gold backing is around 1 ps according to srin calculations [37].

The uncertainty in lifetime measurement is composed of statistical and systematic components. The statistical uncertainty was obtained by evaluating the  $\chi^2$  curve as a function of the lifetime. The difference between  $\chi_{\min}^2$  and  $\chi_{\min}^2 + 1$  was assumed to be statistical uncertainty. The systematic errors have two main sources: the uncertainty in the stopping power at low recoil velocity, and the side feeding effects in the line shape of the transition. The uncertainty due to the stopping power was considered following the prescription suggested by Brandolini *et al.* [30], 8% for lifetimes down to 0.3 ps, and up to 15% below this value. The uncertainty contribution due to the unknown lifetime of the side feeding was estimated using an *a posteriori* method, where, keeping all the other parameters fixed, the side-feeding lifetime was changed until the  $\chi^2$  changed by one unit, and its effect ranged between 0.02 and 0.03 ps for the different states. The results for  $^{47}\text{Cr}$  are presented in Table I.

To ensure the reliability of the method adopted to obtain the lifetimes of  $^{47}\text{Cr}$ , the same procedure was applied to measure the lifetime of the excited states of  $^{47}\text{V}$ . The number of events presented by this reaction channel would allow procedures such as the GTA and the NGTB to be performed, obtaining the lifetimes without the side-feeding contribution to the uncertainty. However, the lifetimes of excited states of the  $^{47}\text{V}$  are well-known, and these different techniques would not be useful to validate the procedure adopted for the less populated  $^{47}\text{Cr}$ . For this reason, an analogous procedure by gating in the lowermost transition of  $^{47}\text{V}$ , 88-keV (5/2<sup>-</sup> → 3/2<sup>-</sup>),

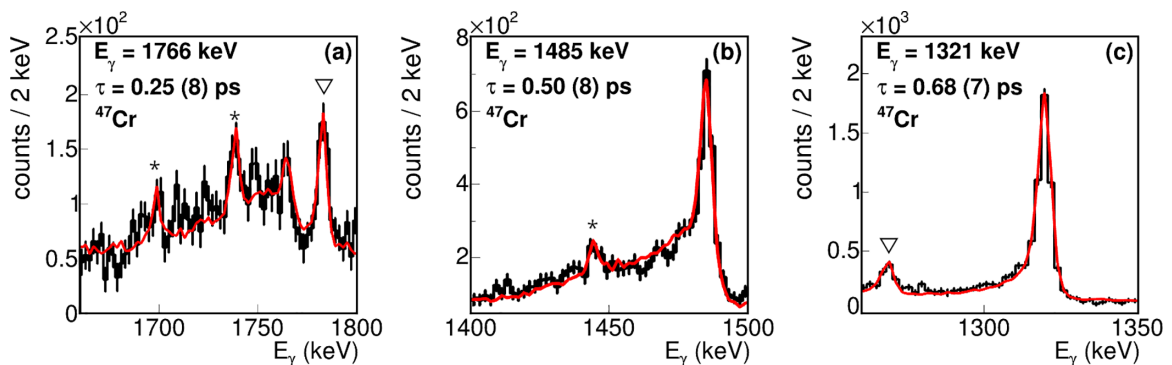


FIG. 2. Line shapes obtained with the AGATA GEANT4 code for Doppler-shifted  $\gamma$ -ray transitions in  $^{47}\text{Cr}$ . The \* symbol denotes unidentified peaks that were included as Gaussian peaks to improve the fit quality. The  $\nabla$  symbol indicates  $\gamma$ -ray transitions belonging to the positive-parity band of  $^{47}\text{Cr}$ , for which no lifetime measurements were performed.

TABLE I. Experimental results obtained for  $^{47}\text{Cr}$ .

Transition	$E_\gamma$ (keV)	$\gamma$ -BR (%)	Intensity (a.u.)	$\tau_{\text{expt.}}$ (ps)	$\tau_{\text{lit.}}^{\text{a}}$ (ps)	$B(E2)_{\text{expt.}}$ ( $e^2 \text{ fm}^4$ )
$(11/2^-) \rightarrow (7/2^-)$	1158	100	196(6)	>3		
$(15/2^-) \rightarrow (11/2^-)$	1321	100	111(5)	0.68(7)	0.84(12)	297(31)
$(19/2^-) \rightarrow (15/2^-)$	1485	100	113(8)	0.50(8)	0.44(6)	225(36)
$(23/2^-) \rightarrow (19/2^-)$	1766	100	52(4)	0.25(8)	<0.64	189(61)
$(3/2^+) \rightarrow (5/2^+)$	372	14 <sup>b</sup>	12(2)			
$(5/2^+) \rightarrow (5/2^-)$	771	7 <sup>b</sup>	3(1)			
$(7/2^+) \rightarrow (5/2^+)$	476	50 <sup>b</sup>	6(1)			
$(7/2^+) \rightarrow (5/2^-)$	1247	13 <sup>b</sup>	18(2)			
$(9/2^+) \rightarrow (5/2^+)$	1087	67 <sup>b</sup>	5(3)			
$(9/2^+) \rightarrow (7/2^+)$	611	5 <sup>b</sup>	2(1)			
$(9/2^+) \rightarrow (7/2^-)$	1782	28 <sup>b</sup>	7(1)			
$(11/2^+) \rightarrow (7/2^+)$	1276	74 <sup>b</sup>	7(2)			

<sup>a</sup>Reference [16].<sup>b</sup>Reference [18].

was performed, and the lifetimes of excited states of  $^{47}\text{V}$  in the sub-picosecond range were determined. The partial level scheme adopted for  $^{47}\text{V}$  is shown in Fig. 1(b). The lifetime of the  $23/2^-$  excited state was obtained using the line shape of the 1770-keV  $\gamma$ -ray, as it is the uppermost observed  $\gamma$ -ray from which an excited state lifetime can be observed with the present data [Fig. 3(a)]. However, the obtained lifetime value can be biased due to the inclusion in the fit of two overlapping transitions of  $^{47}\text{V}$ , 1728-keV ( $17/2^+ \rightarrow 13/2^+$ ) and 1774-keV [ $(19/2^+) \rightarrow 15/2^+$ ], using fixed values found in the literature. The lifetime of the  $19/2^-$  excited state was obtained using the line shape of the 1518-keV  $\gamma$ -ray transi-

tion; the agreement between experimental and simulation can be observed in Fig. 3(b). The lifetime of the  $15/2^-$  excited state was obtained using the line shape of the 1320-keV  $\gamma$ -ray transition and the result can be observed in Fig. 3(c). The lifetime of the  $11/2^-$  excited state was obtained using the line shape of the 1149-keV  $\gamma$ -ray transition; the resulting curve can be observed in Fig. 3(d). The lifetime of the  $9/2^+$  excited state was obtained using the line shape of the 1601-keV  $\gamma$ -ray transition, as it does not overlap with other  $\gamma$ -ray peaks, and the resulting curve can be observed in Fig. 3(e). The lifetime of the  $11/2^+$  excited state was obtained using the line shape of the 668-keV  $\gamma$ -ray transition; the resulting curve can be

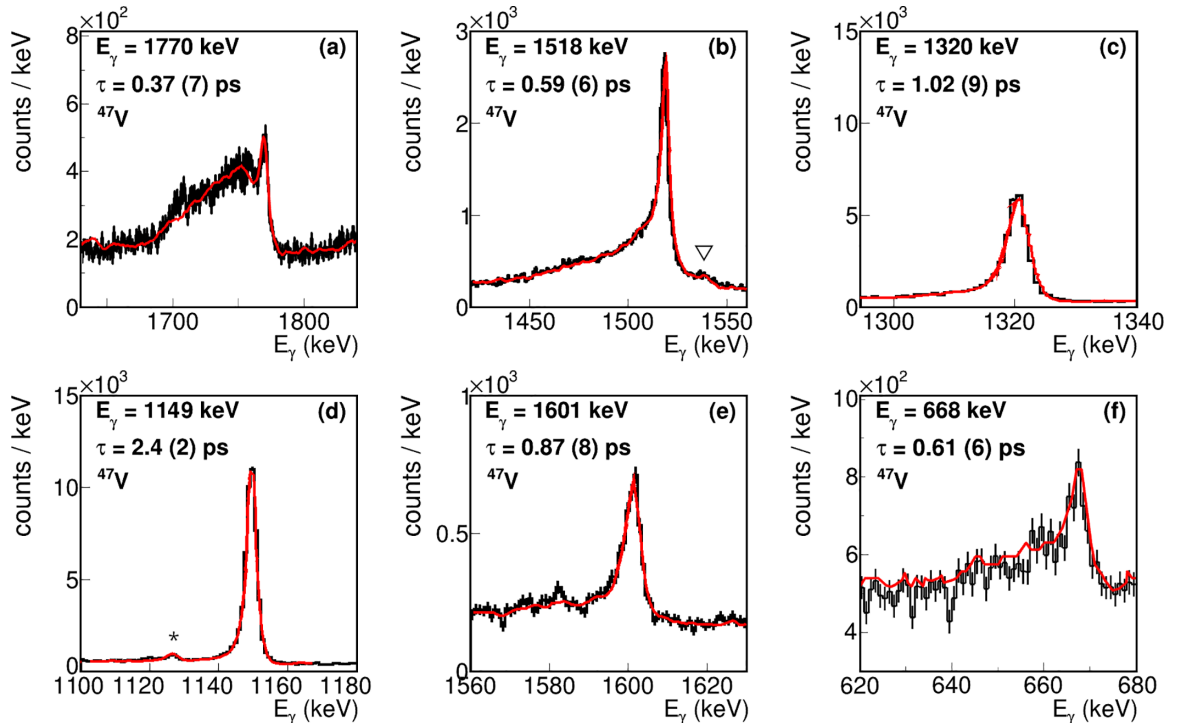


FIG. 3. Line shapes obtained with the AGATA geant4 code for Doppler-shifted  $\gamma$ -ray transitions of  $^{47}\text{V}$ . The \* symbol denotes unidentified peaks that were included as Gaussian peaks to improve the fit quality. The  $\nabla$  symbol indicates the 1539-keV  $\gamma$ -ray transition from  $^{47}\text{V}$ .



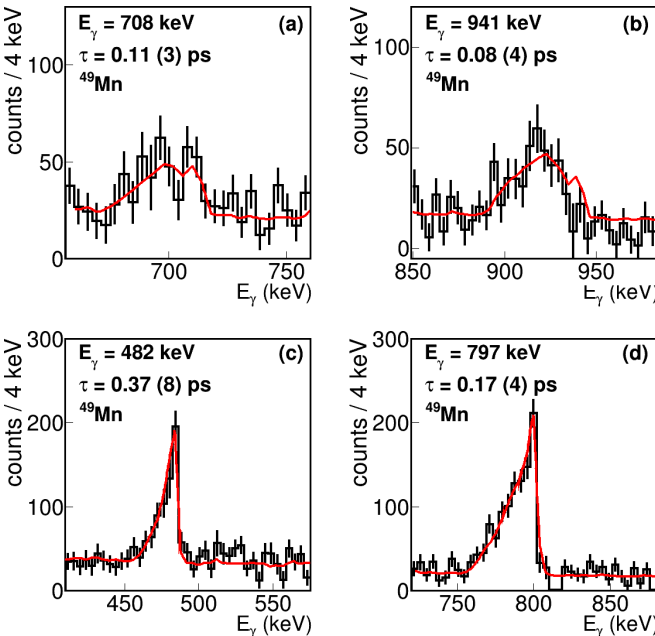
TABLE III. Experimental results obtained for  $^{49}\text{Mn}$ .

Transition	$E_\gamma$ (keV)	$\gamma$ -BR (%)	Intensity (a.u.)	$\tau_{\text{expt.}}$ (ps)	$B(E2)$ ( $e^2 \text{ fm}^4$ )
$9/2^{(-)} \rightarrow 5/2^{(-)}$	1059 <sup>a</sup>	8 <sup>a</sup>	–	0.17(4)	287 <sub>55</sub> <sup>88</sup>
$9/2^{(-)} \rightarrow 7/2^{(-)}$	797	92 <sup>a</sup>	124(15)		
$11/2^{(-)} \rightarrow 7/2^{(-)}$	1279	50 <sup>a</sup>	57(17)	0.37(8)	321 <sub>57</sub> <sup>89</sup>
$11/2^{(-)} \rightarrow 9/2^{(-)}$	482	50 <sup>a</sup>	80(14)		
$13/2^{(-)} \rightarrow 9/2^{(-)}$	1423 <sup>a</sup>	17 <sup>a</sup>	–	0.08(4)	296 <sub>99</sub> <sup>296</sup>
$13/2^{(-)} \rightarrow 11/2^{(-)}$	941	83 <sup>a</sup>	69(17)		
$15/2^{(-)} \rightarrow 11/2^{(-)}$	1649 <sup>a</sup>	41 <sup>a</sup>	–	0.11(3)	249 <sub>53</sub> <sup>93</sup>
$15/2^{(-)} \rightarrow 13/2^{(-)}$	708	59 <sup>a</sup>	36(9)		
$19/2^{(-)} \rightarrow 15/2^{(-)}$	1257	89 <sup>a</sup>	11(8)	>2.1	<110

<sup>a</sup>Reference [17].

same type of procedure as the one applied to the low-statistics channel, a gate in the lowermost transition of  $^{49}\text{Cr}$ , 272-keV ( $7/2^- \rightarrow 5/2^-$ ), was performed, and the lifetimes of excited states of  $^{49}\text{Cr}$  in the sub-picosecond range were determined using the AGATA geant4 code. The partial level scheme adopted for  $^{49}\text{Cr}$  is shown in Fig. 4(b). The lifetime of the  $23/2^-$  excited state was the uppermost observed  $\gamma$ -ray from which an excited state lifetime can be obtained from the line shape of its depopulating 1596-keV  $\gamma$  ray. However, due to the presence of the overlapping 1628-keV  $\gamma$ -ray transition, which depopulates the  $15/2^-$  state, the minimum  $\chi^2$  method presented some limitations. Therefore, a known value from the literature [38] was assigned as the lifetime for the  $23/2^-$  excited state, while the lifetime of the  $15/2^-$  state was determined using the 690-keV  $\gamma$ -ray transition. The resulting curve was an acceptable enough reproduction of the observed experimental line shape, as can be observed in Fig. 6(a). The lifetime of the  $19/2^-$  excited state was obtained using the line

shape of the 1177-keV  $\gamma$ -ray transition. The obtained lifetime is at the limit of what can be measured with the DSAM technique, as shown in Fig. 6(b). The better agreement of the fit with the peak left tail can be a consequence of the inclusion of a more realistic detector response function, which includes the neutron damage. The lifetime of the  $15/2^-$  excited state was obtained using the line shape of the 690-keV  $\gamma$ -ray transition, as it does not overlap with other  $^{49}\text{Cr}$   $\gamma$ -ray transitions. The resulting curve can be observed in Fig. 6(c), where a good agreement was achieved. The lifetime of the  $13/2^-$  excited state was obtained using the line shape of the 938-keV  $\gamma$ -ray transition, as it is the strongest transition depopulating the state, and the resulting curve can be observed in Fig. 6(d). The lifetime of the  $11/2^-$  excited state was obtained using the line shape of the 478-keV  $\gamma$ -ray transition, as it does not overlap with other  $^{49}\text{Cr}$   $\gamma$ -ray transitions, and the resulting curve can be observed in Fig. 6(e). The lifetime of the  $9/2^-$  excited state was obtained using the line shape of the 812-keV  $\gamma$ -ray transition, as it is the strongest transition depopulating the state, and the result can be observed in Fig. 6(f). The results for  $^{49}\text{Cr}$  are compiled in Table IV. The obtained results for  $^{49}\text{Cr}$  are in good agreement with previously reported values in the literature, further validating the employed method.

FIG. 5. Line shapes obtained with the AGATA GEANT4 code for Doppler-shifted  $\gamma$ -ray transitions of  $^{49}\text{Mn}$ .

### III. LARGE-SCALE SHELL-MODEL CALCULATIONS

Shell-model calculations were performed to describe the structure of the studied nuclei. The antoine code was used with the effective interaction KB3G [13], which considers a  $^{40}\text{Ca}$  inert core, and Coulomb matrix elements were added to take into account isospin-breaking effects.

The structure of all isotopes was calculated in the full  $fp$  space. In  $^{49}\text{Mn}$ , the comparison between the experimental and the calculated excitation energies for the natural parity states in Fig. 7 shows good agreement. The shell-model calculations for the isotopes under investigation incorporated high-spin states up to band termination, despite these states not being experimentally populated in the present work. In  $^{47}\text{Cr}$ , the theoretical predictions accurately reproduce the ordering of all states, with the notable exceptions of the  $17/2^-$  and  $19/2^-$  levels that exhibit a deviation from the expected sequence.

The comparison between experimental and shell-model calculations for the electric quadrupole reduced transition

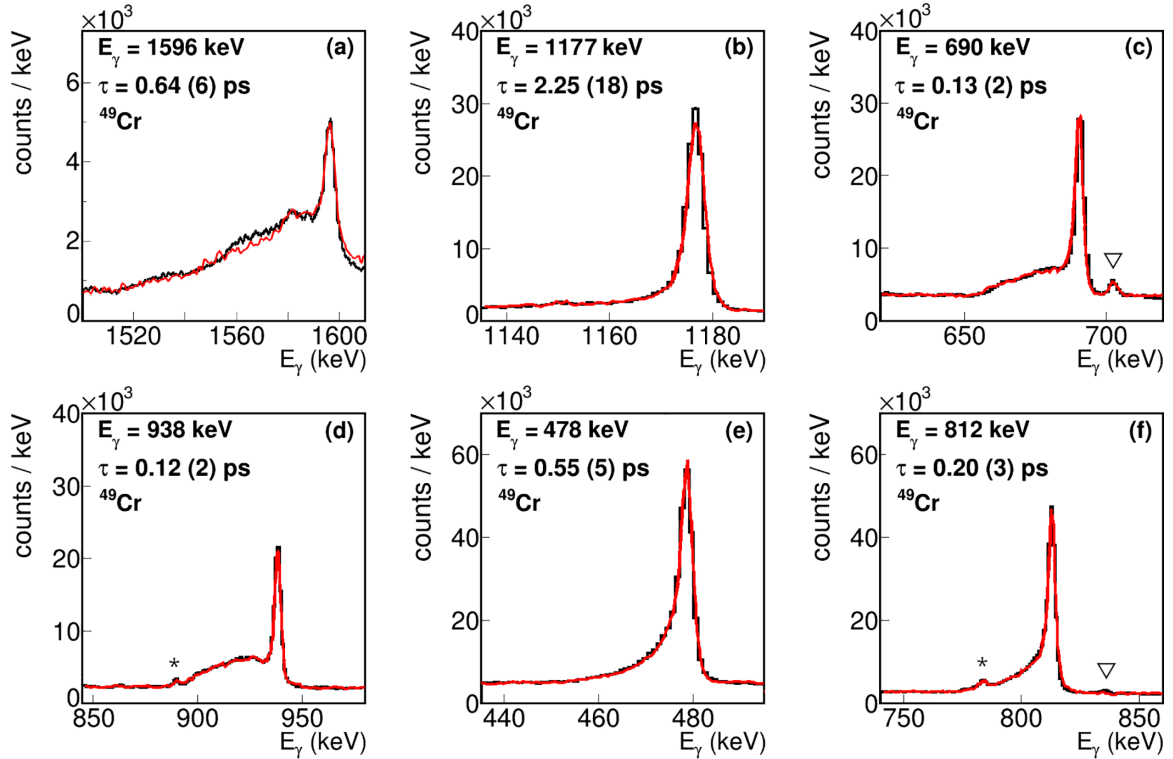


FIG. 6. Line shapes obtained with the AGATA GEANT4 code for Doppler-shifted  $\gamma$ -ray transitions in  $^{47}\text{Cr}$ . The \* symbol denotes unidentified peaks that were included as Gaussian peaks to improve the fit quality. The  $\nabla$  symbol indicates  $\gamma$ -ray transitions belonging to the positive-parity band of  $^{47}\text{Cr}$ , for which no lifetime measurements were performed.

probabilities  $B(E2)$  with the standard adopted values for effective charges with the KB3G interactions  $e_\pi = 1.31e$  and  $e_\nu = 0.46e$  is shown in Fig. 8.

The shell-model-calculated  $B(E2)$  values for  $^{47}\text{Cr}$  are underestimated compared to the experimental ones. However, the general trends are mostly the same, showing a decrease with angular momentum, as is also observed in the

experimental data. The  $B(E2)$  values calculated for  $^{47}\text{V}$  are also underestimated with respect to the experimental values for the  $15/2^-$  and  $19/2^-$  states, but show good agreement for the  $11/2^-$  and  $23/2^-$  states.

In the case of  $^{49}\text{Mn}$ , the shell-model values are in disagreement with the experimental trend, being about three times smaller than the experimental ones for the  $B(E2)$  from

TABLE IV. Experimental results obtained for  $^{49}\text{Cr}$ .

Transition	$E_\gamma$ (keV)	$\gamma$ -BR (%)	Intensity (a.u.)	$\tau_{\text{expt.}}$ (ps)	$\tau_{\text{lit.}}^{\text{a}}$ (ps)	$B(E2)_{\text{expt.}}$ ( $e^2 \text{ fm}^4$ )
$9/2^- \rightarrow 5/2^-$	1084	5(1) <sup>a</sup>	–	0.20(3)	0.22(4)	136(34)
$9/2^- \rightarrow 7/2^-$	812	95(1) <sup>a</sup>	458(2)			
$11/2^- \rightarrow 7/2^-$	1290	54.5(8)	414(9)	0.55(5)	0.57(6)	226(21)
$11/2^- \rightarrow 9/2^-$	478	45.5(8)	345(8)			
$13/2^- \rightarrow 9/2^-$	1416	7.5(9)	24(3)	0.12(2)	0.15(2)	89(18)
$13/2^- \rightarrow 11/2^-$	938	92.5(9)	297(9)			
$15/2^- \rightarrow 11/2^-$	1628	28(2)	91(7)	0.13(2)	0.12(3)	154(26)
$15/2^- \rightarrow 13/2^-$	690	72(2)	232(9)			
$17/2^- \rightarrow 13/2^-$	1718	23(3) <sup>a</sup>				
$17/2^- \rightarrow 15/2^-$	1028	77(3) <sup>a</sup>	52(5)			
$19/2^- \rightarrow 15/2^-$	1177	95(1)	283(8)	2.25(18)	2.1(2)	152(12)
$19/2^- \rightarrow 17/2^-$	149	5(1)	15(3)			
$23/2^- \rightarrow 19/2^-$	1596	100	194(15)		0.64(6)	123(12) <sup>b</sup>

<sup>a</sup>Reference [38].

<sup>b</sup>Calculated using literature  $\tau$  value.

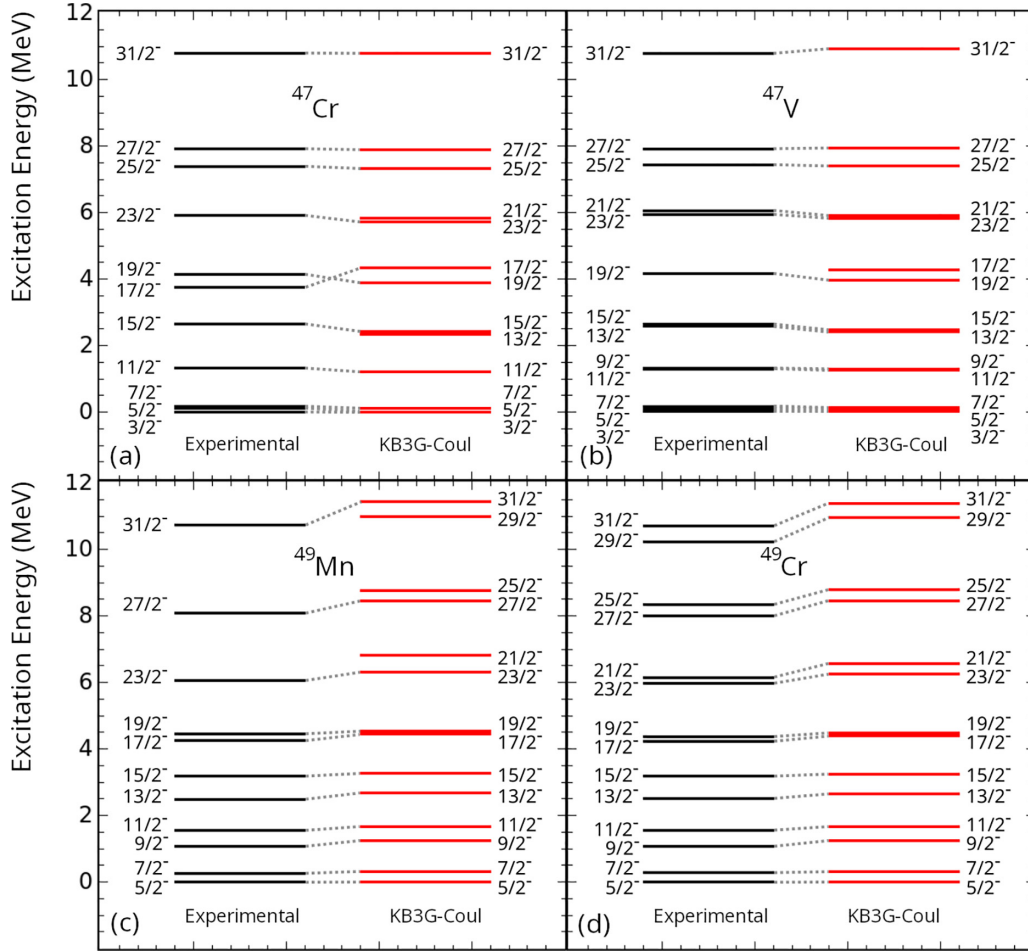


FIG. 7. Comparison between experimental and shell-model-calculated natural parity yrast states for the mirror pairs  $A = 47$  and  $A = 49$ .

the  $9/2^-$ . Such an anomalous behavior is observed in the comparison between theoretical predictions and experimental results. The shell model, despite its well-established success in describing a wide range of nuclear properties in this region, fails in this case to reproduce the experimentally measured data with satisfactory accuracy. The deviation is not a minor fluctuation but rather a systematic discrepancy. In particular, this anomaly cannot be explained in terms of core polarization effects, since the disagreement persists when the calculations are repeated using various sets of effective charges [39]. This persistence suggests that the underlying cause of the anomaly lies beyond the conventional assumptions of the shell model and may point to additional correlations or symmetry-breaking mechanisms that are not properly accounted for within the standard calculation.

The calculation shows a large deficit also for the one from the  $11/2^-$  state. At higher spin, the trend is flatter than the experimental one, but within the error bars. The  $B(E2)$  calculated values for  $^{49}\text{Cr}$  show a better general agreement with the experimental data for higher-spin states. The drop in the experimental value occurring at  $J^\pi = 13/2^-$  might be caused by what is known as band crossing, observed for the same state in  $^{49}\text{Cr}$  in Ref. [38]. Moreover, it is possible to observe that the shell model predicts nearly identical values for the

pair, which have not been verified experimentally. From the experimental point of view, the larger  $B(E2)$  values found for  $^{49}\text{Mn}$  are robust, because even considering that the lifetime values can be affected by systematic errors due to side feeding would have a tendency to overestimate the lifetime. Such a result is surprising, considering that, in this mass region, the shell model can reproduce the values reasonably well, when considering the big differences between the mirror nuclei that have been measured so far. For instance, in the mirror pair  $A = 43$ , the  $B(E2)$  value of the transition  $19/2^- \rightarrow 15/2^-$  in  $^{43}\text{Ti}$  is twice as big as the value in its mirror counterpart, and the shell model can nicely reproduce this difference [40,41].

The transition matrix elements can be decomposed into isoscalar ( $M_0$ ) and isovectorial ( $M_1$ ) components, using Eq. (1):

$$M_p = \frac{1}{2}(M_0 - T_z M_1) = \sqrt{(2J_i + 1)B(E2)}, \quad (1)$$

where the  $B(E2)$  values are the experimental data for each  $J_i$  of a mirror pair [42]. These values were calculated for the excited states in the mirror pairs for which the lifetimes were measured,  $^{47}\text{Cr} - ^{47}\text{V}$  ( $A = 47$ ) and  $^{49}\text{Mn} - ^{49}\text{Cr}$  ( $A = 49$ ), for  $T_z = \pm 1/2$ . The obtained values for the components  $M_0$  are compatible among them within the mirror pair, remaining

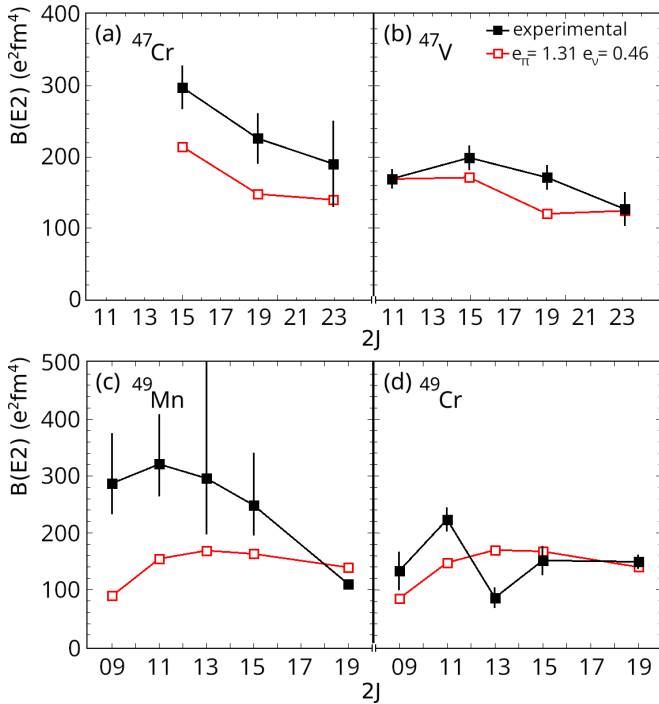


FIG. 8. The experimental and shell-model-calculated reduced transition probabilities  $B(E2)$  for excited states in (a)  $^{47}\text{Cr}$ , (b)  $^{47}\text{V}$ , (c)  $^{49}\text{Mn}$ , where the  $J^\pi = 19/2^{(-)}$   $B(E2)$  value is a superior limit, and (d)  $^{49}\text{Cr}$ .

mostly constant, as can be observed in Fig. 9. A similar result can be observed for the  $M_1$  component, with the values being around  $20 e^2 \text{fm}^2$  for both mirror pairs and zero-compatible when considering the large uncertainty. This indicates that the isoscalar component dominates the transition strength over the isovectorial one.

#### IV. CONCLUSIONS

In this work, we measure the lifetimes of isospin analog excited states in the mirror nuclei  $^{47}\text{Cr} - ^{47}\text{V}$  and  $^{49}\text{Mn} - ^{49}\text{Cr}$  up to 6 MeV. The experiment was performed at the GANIL Laboratory, France, using fusion-evaporation reactions which

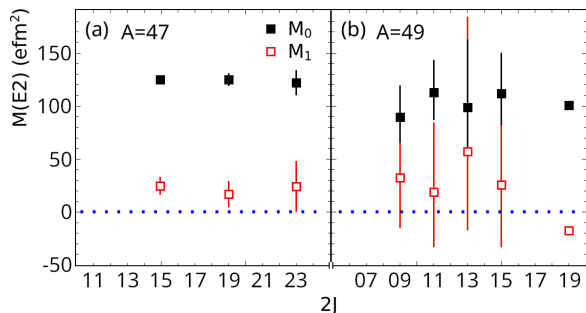


FIG. 9. The  $E2$  matrix transition elements split into isoscalar (black solid squares) and isovector (red empty squares) components. It is possible to observe that the interaction is dominated by the isoscalar component and remains mostly constant within uncertainty.

populated excited states in these nuclei with a heavy-ion beam of  $^{36}\text{Ar}$  at 115 MeV bombarding a target of  $0.55 \text{ mg/cm}^2$  CaO with a gold backing of  $10 \text{ mg/cm}^2$ . The  $\gamma$ -rays depopulating the excited states in these nuclei were detected using the AGATA gamma-ray spectrometer. The charged particles emitted during evaporation were detected by the ancillary detector system DIAMANT, and the neutrons were detected by NEDA, and the neutron wall. The lifetime analysis was performed using realistic line shapes simulated with the AGATA geant4 code. The structure of the nuclei studied in this work was interpreted by comparison to the large-scale shell model with the use of the antoine code and the effective interaction KB3G, which allows the interaction of nucleons in the full  $f p$  space and includes the effects of the Coulomb interaction. While a general agreement is found in the comparison of transition probabilities measured in mirror nuclei with  $A = 47$ , an anomalous behavior is observed for the mirror nuclei with  $A = 49$ . The shell model fails to predict the experimentally measured data, and such an anomaly cannot be ascribed to core polarization since it cannot be recovered employing a different set of effective charges. The decomposition of the transition strength into isoscalar and isovector components indicates that it is dominated by the isoscalar component, remaining constant with the angular momentum.

#### ACKNOWLEDGMENTS

We acknowledge the GANIL facility for the provision of heavy-ion beams and the AGATA Collaboration for the use of the spectrometer. We acknowledge DIAMANT and NEDA Collaborations for instrumental support. Work partially supported by the Coordenação de Aperfeiçoamento de Pessoal de Nível Superior, Brazil (CAPES), Financial code 001, and by the Brazilian funding agencies CNPq (Proc. No. 303295/2022-8) and FAPESP (Proc. No. 2019/07767-1). R.E. also acknowledges the support from the Instituto Nacional de Ciência e Tecnologia de Física Nuclear e Aplicações (INCT-FNA Proc. No. 464898/2014-5). The work is partially supported by MCIN/AEI/10.13039/501100011033, Spain, under Grants No. PID2020-118265GB-C4, No. PID2023-150056NB-C4, No. CEX2023-001292-S, and No. PRTR-C17.I01; by Generalitat Valenciana, Spain, under Grants No. CIPROM/2022/54 and Grant No. ASFAE/2022/031; and by the EU: NextGeneration and FEDER funds. J.B. acknowledges support from Margarita Salas under Grant No. UCM-CT31/21, funded by the Spanish MIU and the EU: Next-Generation funds. R.E., M.A.G., and N.H.M. also acknowledge the support from the Instituto Nacional de Ciência e Tecnologia de Física Nuclear e Aplicações (INCT-FNA, Proc. No. 464898/2014-5).

#### DATA AVAILABILITY

The data that support the findings of this article are not publicly available. The data are available from the authors upon reasonable request.

- [1] E. K. Warburton, *et al.*, *The Role of Isospin in Electromagnetic Transitions* (North-Holland, Amsterdam, 1969).
- [2] G. Morpurgo, Inhibition of  $M1$   $\gamma$  transitions with  $\Delta t = 0$  in self-conjugate nuclei, *Phys. Rev.* **110**, 721 (1958).
- [3] L. A. Radicati, Isotopic spin and Coulomb forces, *Proc. Phys. Soc. A* **66**, 139 (1953).
- [4] M. Gell-Mann, *et al.*, Consequences of charge independence for nuclear reactions involving photons, *Phys. Rev.* **91**, 169 (1953).
- [5] P. Federman and Zamick, State-dependent effective charge in the  $2p-1f$  shell, *Phys. Rev.* **177**, 1534 (1969).
- [6] S. Siegel and L. Zamick, Effective charges for electric multipole transitions, *Phys. Lett. B* **28**, 453 (1969).
- [7] R. du Rietz, *et al.*, Effective charges in the  $fp$  shell, *Phys. Rev. Lett.* **93**, 222501 (2004).
- [8] M. Dufour, *et al.*, Realistic collective nuclear Hamiltonian, *Nucl. Phys. A* **54**, 1641 (1996).
- [9] A. M. Bernstein, *et al.*, Isospin decomposition of nuclear multipole matrix elements from  $\gamma$  decay rates of mirror transitions: Test of values obtained with hadronic probes, *Phys. Rev. Lett.* **42**, 425 (1979).
- [10] B. A. Brown, B. H. Wildenthal, W. Chung, S. E. Massen, M. Bernas, A. M. Bernstein, R. Miskimen, V. R. Brown, and V. A. Madsen, Isovector  $E2$  matrix elements from electromagnetic transitions in the  $s$ - $d$  shell: Experiment and shell-model calculations, *Phys. Rev. C* **26**, 2247 (1982).
- [11] T. K. Alexander, *et al.*, Neutron and proton polarization charges from  $E2$  mirror transitions, *Nucl. Phys. A* **445**, 189 (1985).
- [12] S. R. Stroberg, J. Henderson, G. Hackman, P. Ruotsalainen, G. Hagen, and J. D. Holt, Systematics of  $E2$  strength in the  $sd$  shell with the valence-space in-medium similarity renormalization group, *Phys. Rev. C* **105**, 034333 (2022).
- [13] A. Poves, Shell model study of the isobaric chains  $A = 50$ ,  $A = 51$  and  $A = 52$ , *Nucl. Phys. A* **694**, 157 (2001).
- [14] M. A. Bentley and S. M. Lenzi, Coulomb energy differences between high-spin states in isobaric multiplets, *Prog. Part. Nucl. Phys.* **59**, 497 (2007).
- [15] J. A. Cameron, *et al.*, Mirror nuclei at high spin in the  $f_{7/2}$  shell, *Phys. Lett. B* **319**, 58 (1993).
- [16] D. Tonev, *et al.*, Transition rates and nuclear structure changes in mirror nuclei  $^{47}\text{Cr}$  and  $^{47}\text{V}$ , *Phys. Rev. C* **65**, 034314 (2002).
- [17] J. A. Cameron, *et al.*, Progress in particle and nuclear physics, *Phys. Lett. B* **235**, 239 (1990).
- [18] J. A. Cameron, M. A. Bentley, A. M. Bruce, R. A. Cunningham, W. Gelletly, H. G. Price, J. Simpson, and D. D. Warner, Recoil-separated gamma-ray spectroscopy of  $^{47}\text{Ti}$ ,  $^{47}\text{V}$ ,  $^{47}\text{Cr}$ ,  $^{48}\text{V}$ , and  $^{48}\text{Cr}$ , *Phys. Rev. C* **49**, 1347 (1994).
- [19] C. D. O'Leary, M. A. Bentley, D. E. Appelbe, D. M. Cullen, S. Ertüyyrk, R. A. Bark, A. Maj, and T. Saitoh, Mirror symmetry up to the band termination in  $^{49}\text{Mn}$  and  $^{49}\text{Cr}$ , *Phys. Rev. Lett.* **79**, 4349 (1997).
- [20] M. A. Bentley, S. M. Lenzi, S. A. Simpson, and C. A. Diget, Isospin-breaking interactions studied through mirror energy differences, *Phys. Rev. C* **92**, 024310 (2015).
- [21] S. Akkoyun, *et al.*, AGATA—Advanced GAMMA Tracking Array, *Nucl. Instrum. Methods Phys. Res., Sect. A* **668**, 26 (2012).
- [22] E. Clément, *et al.*, Conceptual design of the AGATA  $1\pi$  array at GANIL, *Nucl. Instrum. Methods Phys. Res., Sect. A* **855**, 1 (2017).
- [23] J. Scheurer, *et al.*, Improvements in the in-beam  $\gamma$ -ray spectroscopy provided by an ancillary detector coupled to a Ge  $\gamma$ -spectrometer: the DIAMANT-EUROGAM II example, *Nucl. Instrum. Methods Phys. Res., Sect. A* **385**, 501 (1997).
- [24] J. Gal, *et al.*, The VXI electronics of the DIAMANT particle detector array, *Nucl. Instrum. Methods Phys. Res., Sect. A* **516**, 502 (2004).
- [25] J. J. Valiente-Dobón, *et al.*, NEDA - NEutron detector array, *Nucl. Instrum. Methods Phys. Res., Sect. A* **927**, 81 (2019).
- [26] O. Skeppstedt, The EUROBALL Neutron Wall — design and performance tests, *Nucl. Instrum. Methods Phys. Res., Sect. A* **421**, 531 (1999).
- [27] O. B. Tarasov, *et al.*, Development of the program LISE: Application to fusion-evaporation, *Nucl. Instrum. Methods Phys. Res., Sect. B* **204**, 174 (2008).
- [28] A. Z. Schwarzschild and E. K. Warburton, The measurement of short nuclear lifetimes, *Annu. Rev. Nucl. Sci.* **18**, 265 (1968).
- [29] D. Branford and I. F. Wright, A Doppler shift attenuation method for measuring lifetimes in the range  $10^{-13} - 10^{-15}$  s using heavy-ion induced reaction, *Nucl. Instrum. Methods* **106**, 437 (1973).
- [30] F. Brandolini, *et al.*, Precise DSAM lifetime measurements in  $^{48}\text{Cr}$  and  $^{50}\text{Cr}$  as a test of large scale shell model calculations, *Nucl. Phys. A* **642**, 387 (1998).
- [31] E. Farnea, *et al.*, Conceptual design and Monte Carlo simulations of the AGATA array, *Nucl. Instrum. Methods Phys. Res., Sect. A* **621**, 331 (2010).
- [32] S. Agostinelli, *et al.*, GEANT4—a simulation toolkit, *Nucl. Instrum. Methods Phys. Res., Sect. A* **506**, 250 (2003).
- [33] J. C. Wells and N. R. Johnson, Lineshape: A computer program for Doppler-broadened lineshape lifetime analysis, Report No. ORNL-6689 44 (ORNL, 1991).
- [34] F. Brandolini and R. V. Ribas, Doppler shift attenuation method analysis with the narrow gate on transitions below procedure, *Nucl. Instrum. Methods Phys. Res., Sect. A* **417**, 150 (1998).
- [35] A. A. Pakou, J. Billowes, A. W. Mountford, and D. D. Warner, Onset of collectivity in the ground-state band of  $^{50}\text{Cr}$ , *Phys. Rev. C* **50**, 2608 (1994).
- [36] H. Hellmeister, *et al.*, Statistical model calculations of continuum feeding times in heavy-ion fusion reactions, *Nucl. Phys. A* **307**, 515 (1978).
- [37] J. F. Ziegler, SRIM-2003, *Nucl. Instrum. Methods Phys. Res., Sect. B* **219-220**, 1027 (2004).
- [38] F. Brandolini, *et al.*, Lifetimes in the middle of  $1f_{7/2}$  shell: Cross-conjugated nuclei  $^{47}\text{V}$  and  $^{49}\text{Cr}$ , *Nucl. Phys. A* **693**, 517 (2001).
- [39] R. Escudeiro, Excited state lifetimes in the  $fp$ -shell mirror nuclei, Ph.D. thesis, Universidade de São Paulo—Università Degli Studi di Padova, 2023.
- [40] R. Hoischen, *et al.*, Isomeric mirror states as probes for effective charges in the lower  $pf$  shell, *J. Phys. G: Nucl. Part. Phys.* **38**, 035104 (2011).
- [41] S. Lenzi (private communication).
- [42] C. Morse, *et al.*, Lifetime measurement of the  $2+$  state in  $^{74}\text{Rb}$  and isospin properties of quadrupole transition strengths at  $N=Z$ , *Phys. Lett. B* **787**, 198 (2018).